Bis(porphyrin)–Anthraquinone Triads: Synthesis, Spectroscopy, and Photochemistry

ARTICLE *in* THE JOURNAL OF PHYSICAL CHEMISTRY A · MARCH 2013

Impact Factor: 2.69

THE JOURNAL OF PHYSICAL CHEMISTRY A

Article

pubs.acs.org/JPCA

Bis(porphyrin)−Anthraquinone Triads: Synthesis, Spectroscopy, and Photochemistry

L. Giribabu,*[,†] P. Silviya Reeta,[†] Ravi Kumar Kanaparthi,[†] Malladi Srikanth,[‡] and Y. Soujanya[‡]

[†]Inorganic & Physical Chemistry Division, CSIR-Indian Institute of Chemical Technology, Hyderabad 500007, A.P., India

[‡]Molecular Modelling Group, Indian Institute of Chemical Technology, Hyderabad 500067, A.P., India

Supporting Information

ABSTRACT: Molecular triads based on bis(porphyrin)−anthraquinone having azomethine bridge at the pyrrole-β position have been designed and synthesized. Both free-base AQ-$(H_2)_2$ and zinc AQ-$(Zn)_2$ triads are characterized by elemental analysis, MALDI-MS, ^{1}H NMR, UV−visible, and fluorescence spectroscopy (steady-state and time-resolved) as well as electrochemical method. The absorption spectra of both Soret and Q-bands of the triads are red-shifted by 12−20 nm with respect to their monomer units. The study supported by theoretical calculations manifests that there exists a negligible electronic communication in the ground state between the donor porphyrin and acceptor anthraquinone of these triads. However, interestingly, both the triads exhibit significant fluorescence emission quenching (51−92%) of the porphyrin emission compared to their monomeric units. The emission quenching is attributed to the excited-state intramolecular photoinduced electron transfer from porphyrins to anthraquinone. The electron-transfer rates (k_{ET}) of these triads are found in the range 1.0×10^8 to 7.7×10^9 s^{-1} and are found to be solvent dependent.

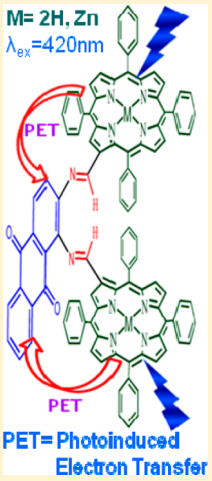

1. INTRODUCTION

Photosynthetic reaction centers, which convert solar energy into useful chemical energy, consist of a protein matrix and donor−acceptor redox active pigments. During photosynthesis, the primary electron-transfer (ET) step occurs from a porphyrin-based complex[1−5] and, subsequently, the excited porphyrin−base complex donates an electron to (bacterio)-chlorophylls or their corresponding dimers and then to bacteriopheophytins and quinone acceptors QA and QB,[6] resulting in a long-lived, charge-separated state. Apart from this, the utmost efficiency with which the chlorophyll−quinone antenna harvest the solar energy has also imparted a special interest in designing a wide variety of efficient porphyrin-based solar cells as well.[7] Numerous model molecules have been reported in the literature for better understanding or mimicking the natural photosynthesis.[8−13]

Covalently/noncovalently linked porphyrin−quinone donor−acceptor (D−A) molecules have been studied extensively as model compounds for the light-induced charge separation step to get insight into the primary event of the natural photosynthesis.[14−18] Many current investigations are concerned with porphyrin−quinone molecules in order to understand the role of distance, orientation, energetic, and medium in determining the rate of intramolecular photoinduced electron transfer (PET).[19,20] Most of these studies mainly employed the *through-space* ($\pi-\pi$ interactions) and/or *through-bond* (superexchange) mechanism. We are particularly interested in the through-bond mechanism because the PET in many D−A systems is known to be dominated by through-bond interactions.[17,21−23] One must note that the spacer between the donor and acceptor plays an important role in the through-bond mechanism. As part of our continuing interest in studying the PET processes,[24−26] here we report the design, synthesis, and spectral (UV−visible, MALDI-MS and ^{1}H NMR) and electrochemical characterization of bis-(porphyrin)−anthraquinone-based molecular triads. Further, photophysical properties of these newly synthesized azomethine-bridged bis(porphyrin)−anthraquinone triad, AQ-$(H_2)_2$, and its zinc derivative, AQ-$(Zn)_2$, have been studied systematically.

2. EXPERIMENTAL SECTION

2.1. Materials. Commercially available reagents and chemicals were used in the present investigations. Analytical reagent grade solvents were used for synthesis, and distilled laboratory-grade solvents were used for column chromatography. Dry chloroform and dichloromethane were prepared by argon-degassed solvent through activated alumina columns. Nitrogen gas (oxygen-free) was passed through a KOH drying column to remove moisture. Neutral alumina (mesh 60−325, Brockmann activity1) was used for column purification. All the reactions were carried out under nitrogen or argon atmosphere

Received: December 10, 2012
Revised: March 19, 2013
Published: March 19, 2013

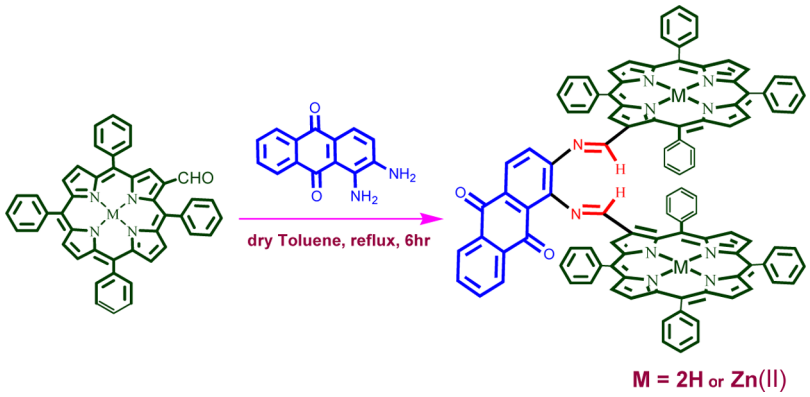

Figure 1. Synthetic scheme of AQ-$(H_2)_2$ and AQ$(Zn)_2$ triads.

using dry degassed solvents and the apparatus was shielded from ambient light.

2.2. Synthesis. 5,10,15,20-Tetraphenylporphyrin (H_2L^1), [5,10,15,20-tetraphenylporphyrinato]zinc(II) (ZnL^1), 2-formyl-5,10,15,20-tetraphenylporphyrin (H_2L^2), and [2-formyl-5,10,15,20-tetraphenylporphyrinato]zinc(II) (ZnL^2) were synthesized as per the reaction procedures reported in the literature.[27,28]

2.2.1. Synthesis of Free Base Triad, AQ-$(H_2)_2$. This compound was synthesized by following Schiff's base reaction. 1,2-Diaminoanthraquinone (71.4 mg, 0.39 mmol) and H_2L^2 (50 mg, 0.07 mmol) were dissolved in 50 mL of dry toluene. The resultant reaction mixture was refluxed for 6 h under inert atmosphere. The solvent toluene was removed under reduced pressure. The obtained solid material was subjected to neutral alumina column and eluted with $CHCl_3$–hexane (8:2%, v/v). The solvent front running band was the unreacted H_2L^2 and the second brown color band was the desired compound. The solvent was removed under vacuum and recrystallized from CH_2Cl_2–hexane to get the desired product in 60% isolated yield. Anal. Calcd. for $C_{104}H_{66}N_{10}O_2$ % (1487.70): C, 83.96; H, 4.47; N, 9.41. Found C, 83.87; H, 4.40; N, 9.35. MALDI-MS (TOF) $[C_{104}H_{66}N_{10}O_2]^+$: 1486 (10%), $[C_{104}H_{66}N_{10}O_2 - C_{46}H_{32}N_4]^{2+}$ 861 (50%). IR: ν_{max} (KBr)/cm^{-1} 3459, 2918, 1652, 1584, 1429, 1275. ^1H NMR ($CDCl_3$, δppm): 9.50 (s, 2H); 8.75–8.88 (m, 12H); 8.16–8.35 (m, 18H,); 7.65–7.86 (m, 24H); 7.60 (m, 2H); 7.52 (m, 2H); 6.75 (d, 2H), and −2.48 (b, 4H).

2.2.2. Synthesis of Zinc Triad, AQ-$(Zn)_2$. This compound was synthesized by following the analogous reaction procedure adopted for AQ-$(H_2)_2$, in which AQ and ZnL^2 were subjected to a condensation reaction. Anal. Calcd. for $C_{104}H_{62}N_{10}O_2Zn_2$ % (1614.45): C, 77.37; H, 3.87; N, 8.68. Found C, 77.47; H, 3.85; N, 8.655. MALDI-MS (TOF) $[C_{104}H_{66}N_{10}O_2Zn - C_{46}H_{32}N_4Zn]^+$: 926 (100%). IR: ν_{max} (KBr)/cm^{-1} 3455, 2929, 1634, 1521, 1278. ^1H NMR ($CDCl_3$, δppm): 9.63 (s, 2H); 8.83–8.99 (m, 12H); 8.16–8.35(m, 18H,); 7.68–7.89 (m, 24H); 7.49 (m, 2H); 7.43 (m, 2H); 6.66 (d, 2H).

2.3. Methods and Instrumentation. ^1H NMR spectra were recorded on a 500 MHz INOVA spectrometer. Cyclic and differential-pulse voltammetric measurements were performed on a PC-controlled electrochemical analyzer (CH instruments model CHI620C). All these experiments were performed with 1 mM concentration of compounds in dichloromethane at a scan rate of 100 mV s^{-1} in which tetrabutylammonium perchlorate (TBAP) is used as a supporting electrolyte as documented in our previous reports.[29]

2.3.1. Theoretical Calculations. Full geometry optimization computations of the AQ-$(H_2)_2$ and AQ-$(Zn)_2$ triads were carried out with the DFT-B3LYP method using 6-31G* basis set and frequency analysis confirmed that the obtained geometries are to be genuine global minimum structures. All calculations were performed with the Gaussian G03 (d01) package on a personal computer.[30]

2.3.2. Absorption and Fluorescence Measurements. The optical absorption spectra were recorded on a Shimadzu (Model UV-3600) spectrophotometer. Concentrations of solutions are ca. 1×10^{-6} M (porphyrin Soret band) and 5×10^{-5} M (porphyrin Q-bands). Steady-state fluorescence spectra were recorded on a Fluorolog-3 spectrofluorometer (Spex model, Jobin Yvon) for solutions with optical density at the wavelength of excitation (λ_{ex}) ≈0.05. Fluorescence quantum yields (ϕ) were estimated by integrating the fluorescence bands and by using either [H_2L^1] (ϕ = 0.13 in CH_2Cl_2) or [ZnL^1] (ϕ = 0.036 in CH_2Cl_2) as reference compound.[31] Fluorescence lifetime measurements were carried on a picosecond time-correlated single-photon-counting (TCSPC) setup (FluoroLog3-Triple Illuminator, IBH Horiba Jobin Yvon) employing a picosecond light-emitting diode laser (NanoLED, λ_{ex} = 405 nm) as excitation source. The decay curves were recorded by monitoring the fluorescence emission maxima of the triads (λ_{em} = 650 nm). Photomultiplier tube (R928P, Hamamatsu) was employed as the detector. The lamp profile was recorded by placing a scatterer (dilute solution of Ludox in water) in place of the sample. The width of the instrument response function (IRF) was limited by the full width at half-maximum (fwhm) of the excitation source, ~625 ps at 405 nm. Decay curves were analyzed by nonlinear least-squares iteration procedure using IBH DAS6 (version 2.3) decay analysis software. The quality of the fits was judged by the χ^2 values and distribution of the residuals.

3. RESULTS AND DISCUSSION

Both the triads AQ-$(H_2)_2$ and AQ$(Zn)_2$ were synthesized by using Schiff base condensation reaction as shown in Figure 1. The desired compounds were obtained with moderate yields (~60%) in both cases after column chromatography purification and subsequent recrystallization. Preliminary characterization of both the triads was carried out by MALDI-TOF MS and UV–visible spectroscopic methods. The mass spectrum of AQ-$(H_2)_2$ showed a peak at m/z = 1486 ($[M]^+$, $C_{104}H_{66}N_{10}O_2$) ascribable to the molecular-ion peak. The subsequent peak at m/z = 861 can be ascribed to the detachment of one ($[M-C_{104}H_{66}N_{10}O_2-C_{46}H_{32}N_4]^{2+}$ free-base

dx.doi.org/10.1021/jp312134a | J. Phys. Chem. A 2013, 117, 2944–2951

porphyrin subunit from the triad. A similar type of fragmentation was also observed in the case of AQ-$(Zn)_2$. The stretching peak at 1548 and 1521 cm^{-1} in the IR spectra of AQ-$(H_2)_2$ and AQ-$(Zn)_2$, respectively, confirms the presence of the C═N bond in both the triads (Figures S1 and S2 in the Supporting Information).

^{1}H NMR spectral data of both the triads have been summarized in the Experimental Section and the spectra of AQ-$(H_2)_2$ and AQ-$(Zn)_2$ are shown in Figure 2. Comparison of these spectra with those of individual constituents (H_2L^1, ZnL^1, and AQ) reveals that there is no appreciable change in resonance positions of various protons present in the porphyrin macrocycle and that of the anthraquinone part of the triad AQ-$(H_2)_2$, whereas in the case of AQ-$(Zn)_2$, a subtle shift of protons probably due to the interaction of the anthraquinone part of the triad with zinc porphyrin is observed.[17] This is reasonable if one considers that the two aromatic rings are in *trans* configuration with respect to the C═N spacer, avoiding steric interaction. This is confirmed by energy minimization study of the triads which is discussed in section 3.3.

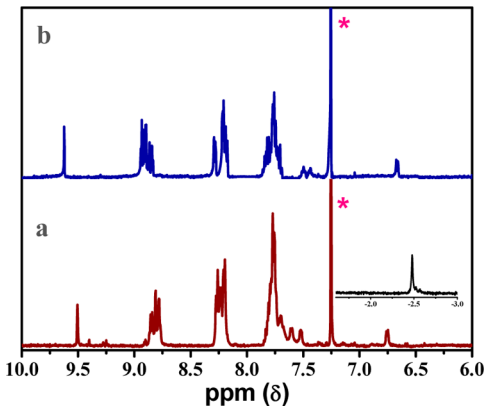

Figure 2. ^{1}H NMR spectra of (a) AQ-$(H_2)_2$ and (b) AQ-$(Zn)_2$ in $CDCl_3$. The peak labeled with asterisk (*) is due to solvent.

3.1. Ground-State Properties. Electronic absorption profiles of AQ-$(H_2)_2$ and AQ-$(Zn)_2$ have been measured in CH_2Cl_2, and the spectral behavior is compared with individual monomer units, H_2L^1 and ZnL^1 (Figure 3). Spectroscopic data which include wavelength of maximum absorbance (λ_{max}), molar extinction coefficients (log ε) of both triads, and their constituent individual components are summarized in Table 1. As shown in Figure 3, the absorption spectrum is a combination of constituent porphyrin and anthraquinone. Both triads exhibit characteristic intense Soret band (~430 nm), which is an $a_{1u}(\pi)/e_g(\pi^*)$ electronic transition, assigned to the second excited state (S_2) and Q-bands (500−700 nm) originated from $a_{2u}(\pi)/e_g(\pi^*)$ electronic transition, attributed to the first excited state (S_1). These characteristic bands are similar to many other dimers or trimers.[32,33] The band centered at ~260 nm is largely due the anthraquinone moiety as the porphyrins have very limited/poor absorption in that region (230−350 nm). It is also observed that the bands are red-shifted and slightly broadened compared to simple H_2L^1 and ZnL^1 porphyrin units. Similar such red shifts and broadening were observed in other pyrrole-β substituted porphyrins as well.[28,34,35] This spectral red shift (20−30 nm) can be explained based on the extended π-electron conjugation of the porphyrin unit to the anthraquinone, and from there to the other porphyrin unit through the two imine (−C═N−) links. The broadening is more pronounced at the longer wavelength region (>600 nm) which might be due to charge or electron transfer because of donor−acceptor−donor type of molecular arrangement. However, that the spectral broadening does not affect further with the solvent polarity indicates the lack of ground-state charge or electron transfer (Figure S9 in the Supporting Information). So, the broadening which we observe perhaps is due to conformers originated from the different orientations of porphyrin units around the two −C−N− bonds.[36]

Figure 4 illustrates the differential pulse voltammograms of AQ, AQ-$(H_2)_2$, and AQ-$(Zn)_2$, and Table 1 summarizes the redox potential data (CH_2Cl_2 and 0.1 M TBAP) of the D_2−A systems investigated in this study along with that of the corresponding individual constituents. Figure 4 and data in Table 1 indicate that each new compound investigated shows three reduction peaks and two oxidation peaks under the experimental conditions employed in this study. Wave analysis suggested that, in general, while the first two reduction steps and first two oxidation steps are reversible (i_{pc}/i_{pa} = 0.9−1.0) and diffusion-controlled ($i_{pc}/\nu^{1/2}$ = constant in the scan rate (ν) range 50−500 mV/s) one-electron transfer (ΔE_p = 60−70 mV; ΔE_p = 65 ± 3 mV for ferrocenium/ferrocene couple) reactions, the subsequent steps are, in general, either quasi-reversible ($E_{pa} - E_{pc}$ = 90−200 mV and i_{pc}/i_{pa} = 0.5−0.8 in the scan rate (ν) range 100−500 mV s^{-1}) or totally irreversible. The peaks occurring at anodic potentials are ascribed to successive one-electron oxidations of the porphyrin parts of AQ-$(H_2)_2$ and

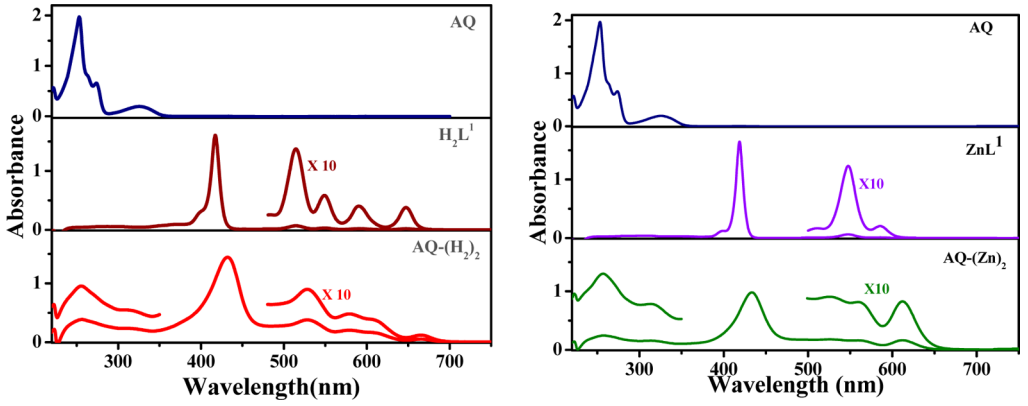

Figure 3. Absorption behavior of AQ, H_2L^1, AQ-$(H_2)_2$, ZnL^1, and AQ-$(Zn)_2$ in CH_2Cl_2.

dx.doi.org/10.1021/jp312134a | J. Phys. Chem. A 2013, 117, 2944−2951

Table 1. UV−Visible and Electrochemical Data of AQ, H_2L^1, AQ-$(H_2)_2$, and AQ-$(Zn)_2$

	absorption, λ_{max}, nm (log ε, M^{-1} cm^{-1})[a]						potential, V vs SCE[b]	
compd	porphyrin bands					AQ bands	reduction	oxidation
H_2L^1	416 (6.06)	515 (4.27)	549 (3.90)	592 (3.77)	646 (3.69)	–	−1.22, −1.56	1.01, 1.25
ZnL^1	419 (6.17)	547 (4.34)	586 (3.60)			–	−1.45, −1.71	0.72, 1.06
AQ		–				256 (7.40)	−0.96, −1.38	–
AQ-$(H_2)_2$	433 (5.40)	527 (4.69)	580 (4.39)	608 (4.34)	668 (3.77)	257 (4.91)	−0.86, −1.10, −1.50	1.00, 1.27
AQ-$(Zn)_2$	434 (5.6)	526 (4.72)	560 (4.71)	613 (4.72)		257 (4.90)	−0.83, −1.28, −1.54	0.89, 1.21

[a]Solvent CH_2Cl_2. Error limits: λ_{max}, ±1 nm; log ε, ±10%. [b]CH_2Cl_2, 0.1 M TBAP. Glassy carbon working electrode; standard calomel electrode is reference electrode, Pt electrode is auxiliary electrode. Error limits, $E_{1/2}$ ± 0.03 V.

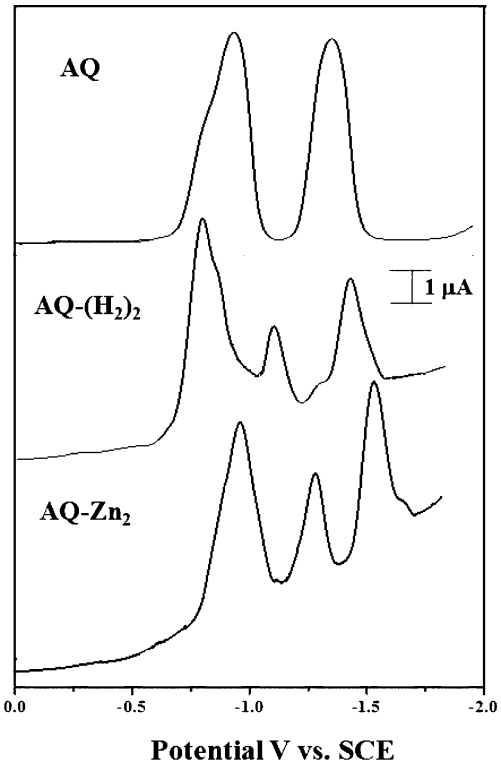

Figure 4. Differential pulse voltammograms of AQ, AQ-$(H_2)_2$, and AQ-$(Zn)_2$ in CH_2Cl_2 with 0.1 M TBAP.

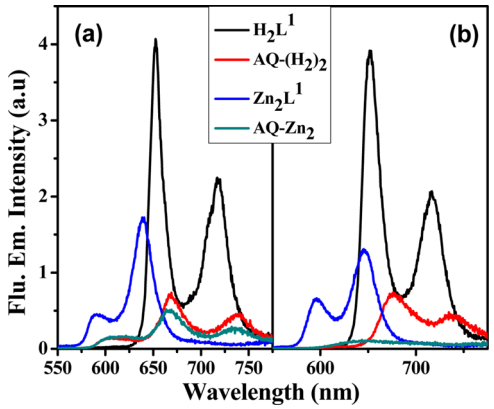

Figure 5. Fluorescence spectra (λ_{ex}= 420 nm) of equiabsorbing solutions of H_2L^1, ZnL^1, AQ-$(H_2)_2$, and AQ-$(Zn)_2$ (OD λ_{ex} = 0.05) in cyclohexane (a) and CH_2Cl_2 (b).

AQ-$(Zn)_2$. As seen in Figure 4, the differential pulse voltammograms of AQ-$(H_2)_2$ and AQ-$(Zn)_2$ in CH_2Cl_2 contain three reduction peaks corresponding to the reduction of porphyrins (H_2/Zn)/anthraquinone moiety. Comparing the reduction potentials of AQ-$(H_2)_2$ and AQ-$(Zn)_2$ with their reference compounds AQ, H_2L^1, and ZnL^1, it was found that the reduction potentials for the first peak purely belongs to the reduction of anthraquinone part of both the triads. The second reduction belongs to the first reduction of porphyrin moiety and third reduction peak belongs to the second reduction of porphyrin and anthraquinone of the D_2−A systems.

The spectroscopic and electrochemical features described above suggest that, in the ground state, electronic communication between porphyrin and anthraquinone chromphores is quite negligible in these new D−A systems. More importantly, one can exploit the excited-state properties by selective excitation of the individual chromophore units.

3.2. Singlet-State Properties. Figure 5 illustrates the steady-state fluorescence spectra of AQ-$(H_2)_2$ and AQ-$(Zn)_2$ triads along with their individual constituents H_2L^1 and ZnL^1 measured in cyclohexane and dichloromethane (CH_2Cl_2). The corresponding emission maxima and quantum yields have been collected in Table 2. The fluorescence emission maxima of free base AQ-$(H_2)_2$ and AQ-$(Zn)_2$ are red-shifted ∼25 and ∼4 nm, respectively, with respect to isolated free base porphyrin and zinc porphyrin units. A similar red shift in emission maxima was also observed in other pyrrole-β substituted porphyrins.[34,35] The red shift of these triads is due to the more polar nature of the emitting state originated from the donor−acceptor−donor (D−A−D) type molecular arrangement in which the anthraquinone is the acceptor and porphyrin acts as donor. Interestingly, we observe remarkable decrease in porphyrin emission intensity when equiabsorbing solutions of triads were excited at 420 nm (λ_{max}, where prophyrin absorbs predominantly). The posibility of self-aggregation of porphyrins which leads to quenching of fluorescence intensity (as a result of nonradiative path in the excited state) can be ruled out as all experiments were carried out with very dilute solutions (10^{-6} M). Moreover, we could not observe substantial changes in the absorption spectra as it happens in few porphyrin systems.[37]

The excited-state energy transfer (EET) or photoinduced electron transfer (PET) could also be responsible for the decrease in fluorescence intensity. For EET, the emission spectra of the donor has to be well matched with the absorption of the acceptor. It is evident from the Figures 3 and 5 that the EET is not possible between anthraquinone and porphyrin due to lack of proper spectral overlap. Alternative pathway for emission quenching is the intramolecular PET from the singlet state of the porphyrin donor to the ground state of the anthraquinone acceptor. The E_{0-0} (0−0 spectroscopic transition energy) values of porphyrin part of triads, 1.86 ± 0.05 eV and 1.96 ± 0.05 eV for AQ-$(H_2)_2$ and AQ-$(Zn)_2$, respectively, as estimated from overlap of their absorption and emission

dx.doi.org/10.1021/jp312134a | J. Phys. Chem. A 2013, 117, 2944−2951

Table 2. Fluorescence Data[a]

compound	λ_{em}, nm (ϕ, %Q)[b] cyclohexane	toluene	CH_2Cl_2	CH_3CN
		λ_{ex} = 420 nm		
H_2L^1	653, 719 (0.122)	653, 719 (0.137)	652,716 (0.130)	651,716 (0.130)
ZnL^1	595, 642 (0.037)	598, 647 (0.046)	646, 596 (0.036)	657, 603 (0.048)
AQ-$(H_2)_2$	671, 742 (0.044, 64)	674, 740 (0.042, 69)	676,738 (0.035, 75)	675, 737 (0.015, 89)
AQ-$(Zn)_2$	670,737 (0.020, 51)	674, 737 (0.022, 52)	651 (0.005, 86)	675, 739 (0.004, 92)

[a]Error limits: λ_{ex}, ±2 nm; ϕ, ±10%. [b]Q is defined in eq 2 (see text).

spectra were found to be in the same range as the E_{0-0} values of free H_2L^1/ZnL^1.[38] The change in free energy for PET from the porphyrin to the anthraquinone can be calculated using the equation

$$\Delta G(^1\text{Por} \rightarrow \text{AQ}) = E_{CT}(\text{Por}^+\text{AQ}^-) - E_{0-0}(\text{Por}) \quad (1)$$

ΔG was found to be −0.096 and −0.24 eV for AQ-$(H_2)_2$ and AQ-$(Zn)_2$, respectively, when excited at 420 nm. This ΔG clearly indicates that there could be a possibility of PET from free base/metal porphyrin to anthraquinone.

Fluorescence quantum yields of the triads and individual constituents have been estimated (Table 2) by comparing the emission curves of reference compounds (i.e., H_2L^1 or ZnL^1, ϕ = 0.13 ± 0.01 and 0.036 ± 0.001, respectively, in CH_2Cl_2 solvent) with those of the triads. It was found that the fluorescence quantum yields (ϕ) of AQ-$(H_2)_2$ and AQ-$(Zn)_2$ are 0.042 and 0.022, respectively, in CH_2Cl_2 solvent. The quenching efficiency values (Q) can be estimated from

$$Q = \frac{\phi(H_2L^1) \text{ or } (ZnL^1) - \phi[\text{AQ-}(H_2)_2] \text{ or } [\text{AQ-}(Zn)_2]}{\phi(H_2L^1) \text{ or } (ZnL^1)} \quad (2)$$

where $\phi(H_2L^1)/(ZnL^1)$ and ϕ(AQ-$(H_2)_2$/AQ-$(Zn)_2$) refer to the fluorescence quantum yields of H_2L^1/ZnL^1 and the triads, respectively; (λ_{ex} = 420 nm). As the static dielectric constant of the solvent is increased, the fluorescence quantum yield decreased gradually (Table 2), indicating the excited-state electron-transfer mechanism. For example, quenching efficiencies in cyclohexane and toluene are less compared to CH_2Cl_2 and CH_3CN. In general, the PET process is accelerated by polar solvents than the nonpolar solvents, and so the present results are consistent with the literature.[39] Efficient quenching of the AQ-$(Zn)_2$ triad relative to that of the AQ-$(H_2)_2$ can be directly attributed to the more exothermic value of ΔG_{PET} of AQ-$(Zn)_2$.

Further evidence of the intramolecular PET process has been evaluated by measuring the excited-state decay curves. Figure 6 illustrates excited-state decay curves of triads, collected in CH_2Cl_2 solvent upon excitation at 405 nm, and the decay parameters collected in four different solvents are shown in Table 3. From the data, it is clear that the fluorescence lifetimes τ (λ_{ex} = 405 nm and λ_{em} = 650 nm) of both AQ-$(H_2)_2$ and AQ-$(Zn)_2$ are decreased in all solvents when compared to H_2L^1/ZnL^1. In all solvents, AQ-$(H_2)_2$ decay curves are fitted with a triexponential expression and the major component has shorter lifetime which is attributed to the deactivation (quenching) of the excited porphyrin by anthraquinone.[17] The other two lifetime components are assigned either to an unquenched decay or decay of the porphyrin−hydroquinone generated by porphyrin-sensitized photoreduction[40] and different conformers of the molecule with flexible linker in solution state.[41,42] On

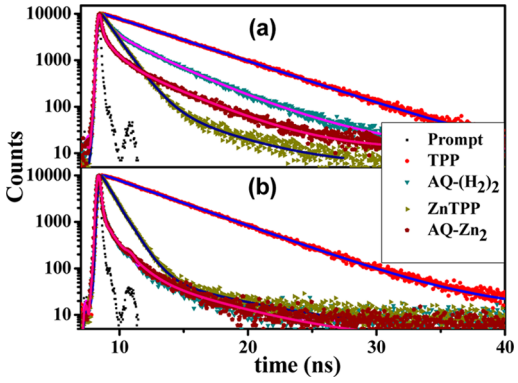

Figure 6. Fluorescence decay (λ_{ex} = 405 nm, λ_{em} = 650 nm) in cyclohexane (a) and CH_2Cl_2 (b).

Table 3. Fluorescence Decay Parameters[a] **and Electron-Transfer Rate Constants (k_{ET}, s^{-1})**[b]

compound	τ, ns (A, %), k_{ET}, s^{-1} cyclohexane	toluene	CH_2Cl_2	CH_3CN
H_2L^1	9.47	9.71	8.81	9.40
ZnL^1	1.93 (93)	2.07 (95)	1.76 (95)	1.72 (89)
	2.07 (7)	1.11 (5)	1.17 (5)	2.86 (11)
AQ- $(H_2)_2$	1.07 (44)	3.08 (57)	0.13 (66)[c]	0.69 (57)
	9.12 (35)	9.26 (23)	6.36 (12.0)	7.60 (32)
	5.14 (21)	4.60 (20)	1.57 (22)	2.28 (11)
	8.3×10^8	2.2×10^8	7.6×10^9	1.3×10^9
AQ-Zn_2	1.60 (85)	1.48 (68)	0.33 (65)[c]	0.60 (51)
	1.16 (6)	2.04 (11)	2.46 (13)	1.82 (26)
	0.57 (9)	0.29 (21)[c]	1.22 (22)	1.00 (23)
	1.0×10^8	1.9×10^8	2.4×10^9	1.1×10^9

[a]All lifetimes are in nanoseconds (ns). [b]Error limits of τ and k_{ET} ~10%. Values in parentheses are relative amplitudes of the corresponding decay components. [c]These short lifetime components are limited by the instrument response function (IRF).

the other hand, AQ-$(Zn)_2$ decay curves are fitting into a three-exponential expression composed of one major (see Table 3, shorter lifetime) component and two minor components (shorter and longer lifetime). From this data, the shorter lifetimes with higher amplitude and longer lifetime components have the same origin as in AQ-$(H_2)_2$, but the additional shorter lifetime component may be due to the noncovalent interaction of the oxygen lone pair of electrons (anthraquinone) with zinc metal present in other porphyrin of AQ-$(Zn)_2$. We believe that this anthraquinone-ligated state is responsible for the additional short-lived component obtained from the TCSPC experiments.[17] In all four investigated solvents, it is observed that the shorter lifetimes of AQ-$(H_2)_2$ have much larger amplitudes

relative to the longer lifetime components. Similar features are also seen in the AQ-$(Zn)_2$ triad.

Further, rate constants (k_{ET}) for the charge-transfer state $Por^{\bullet+}AQ^{\bullet-}$ have been calculated using eq 3 and and summarized in Table 3.

$$k_{ET} = (1/t_f) - k \quad (3)$$

where k is the reciprocal of the lifetime of the H_2L^1/ZnL_1 and τ_f is the lifetime of AQ-$(H_2)_2$/AQ-$(Zn)_2$. The solvent-dependent k_{ET} values are in the range of 1.0×10^8 to 7.7×10^9 s^{-1}. The observed general increase of the k_{ET} values with increasing polarity of the solvent is consistent with the participation of a charge-transfer state in the excited-state deactivation of the porphyrin components of these D_2−A systems. Figure 7 shows

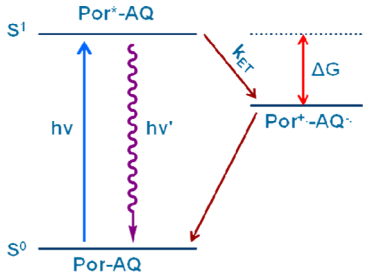

Figure 7. Photoinduced electron-transfer scheme of bis(porphyrin)−anthraquinone triads.

the energy levels of the porphyrin singlet excited state and the charge-transfer state that participate in the PET processes in bis(porphyrin)−anthraquinone triads. In order to establish the intramolecular PET process of these two triads, we have carried out computational calculations to generate frontier molecular orbitals of both triads.

3.3. Theoretical Calculations. In general, intramolecular electron transfer operates by either through-space or through-bond mechanism. In the former mechanism (through space), electron transfer occurs from HOMO (the highest occupied molecular orbital) of the donor moiety to LUMO (the lowest unoccupied molecular orbital) of the acceptor moiety when they are in close proximity and depends strongly on the orientation of donor and acceptor moieties.[43,44] The latter mechanism (through bond) is rather less sensitive to geometrical position/orientation of donor and acceptor moieties but strongly depends on the number of atoms connecting them. In this case, electronic states of spacer (moieties between the donor and the acceptor) will mix with those of the donor and acceptor, and thus the through-bond mechanism is synonymous with superexchange.[45,46] In order to examine the nature and position of frontier molecular orbitals, density functional theory (DFT) calculations have been carried out. Complete optimization without any constraint was done using B3LYP and 6-31g(d) basis set to see the structural parameters of the two systems, AQ-$(H_2)_2$ and zinc AQ-$(Zn)_2$.

Figure 8 displays the HOMO and LUMO distribution and geometrical optimized structures of the triads AQ-$(H_2)_2$ and AQ-$(Zn)_2$, obtained by DFT calculations. From Figure 8, it is clear that the HOMO is mainly distributed at the porphyrin moiety while LUMO is mainly distributed at the anthraquinone moiety. The energies of HOMO and LUMO for triads AQ-$(H_2)_2$ and AQ-$(Zn)_2$ were found to be −4.958 and −5.054 eV and −2.578 and −2.511 eV, respectively. From the geometrical optimized structures (Figure 8), the two porphyrin rings are

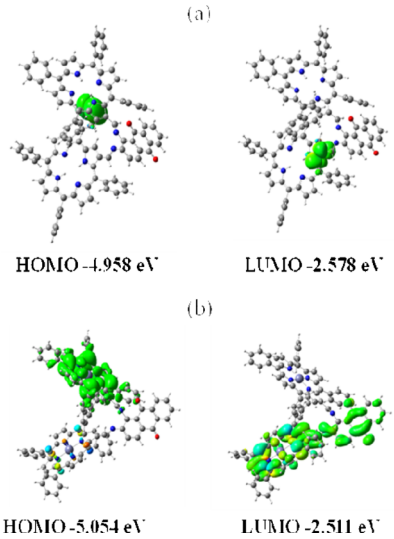

Figure 8. Frontier molecular orbitals, HOMO and LUMO, of (a) AQ-$(H_2)_2$ and (b) AQ-$(Zn)_2$ optimized at the B3LYP/6-31G(d) level.

away from each other as the connecting bonds between porphyrin ring and anthraquinone moieties are not long enough to have $\pi-\pi$ interaction. Similarly, the porphyrin and anthraquinone rings are also far apart which clearly suggests that there is very less chance to have facial interaction between donor porphyrin and acceptor anthraquinone. Moreover, phenyl rings at *-meso* positions are found to be perpendicular to the plane of the porphyrin ring, which prevents the stacking interaction. (All these observations corroborate the prevalence of through-bond intramolecular electron-transfer mechanism in the current systems.) As discussed in earlier sections, the fluorescence quantum yields, lifetimes, and electron-transfer rates of these triads are found to be strongly dependent on solvent polarity. One cannot expect this solvent dependency if electron transfer occurs via the through-space mechanism. Therefore, the results are best compatible with the "through-bond" mechanism for electron-transfer pathway.

4. CONCLUSIONS

In conclusion, bis(porphyrin)−anthraquinone triads having azomethine-bridge at pyrrole-β position of porphyrin macrocycle were successfully shown to be a model photosynthetic reaction center to simulate electron transfer from chlorophylls to the electron acceptors. The ground-state properties indicate that there are no interactions between porphyrin macrocycles and anthraquinone moieties in both the triads. Steady-state and time-resolved spectroscopy showed that AQ-$(H_2)_2$ and AQ-$(Zn)_2$ undergo rapid intramolecular electron transfer from singlet state of porphyrin to anthraquinone. The electron-transfer rates are found in the range 1.0×10^8 to 7.7×10^9 s^{-1} and are solvent dependent.

■ ASSOCIATED CONTENT

Ⓢ Supporting Information

Characterization data of the compounds such as IR spectra (Figures S1 and S2), ^{1}H NMR (Figures S3, S4, S5, and S6), MALDI-MS spectra (Figures S7 and S8), and absorption spectra of AQ-$(H_2)_2$ in different solvents (Figure S9); fluorescence behavior of the compounds in toluene and acetonitrile (Figures S10 and S11); fluorescence decay curves (Figures S12 and S13); and optimized geometries of molecules

dx.doi.org/10.1021/jp312134a | J. Phys. Chem. A 2013, 117, 2944−2951

(Figure S14). This material is available free of charge via the Internet at http://pubs.acs.org.

AUTHOR INFORMATION

Corresponding Author

*E-mail: giribabu@iict.res.in. Phone: +91-40-27191724. Fax: +91-40-27160921.

Notes

The authors declare no competing financial interest.

ACKNOWLEDGMENTS

We are grateful to the Department of Science and Technology (DST, SR/S1/IC21/2008) for financial support of this work. P.S. is thankful to the CSIR for the fellowship. Y.S. thanks BRNS (DAE) for financial support.

REFERENCES

(1) Kim, J. H.; Lee, M.; Lee, J. S.; Park, Ch. B. Self-Assembled Light-Harvesting Peptide Nanotubes for Mimicking Natural Photosynthesis. *Angew. Chem., Int. Ed.* **2012**, *51*, 517−520.

(2) McConnell, I.; Li, G.; Brudvig, G. W. Energy Conversion in Natural and Artificial Photosynthesis. *Chem. Biol.* **2010**, *17*, 434−447.

(3) Gust, D.; Moore, T. A.; Moore, A. L. Solar Fuels via Artificial Photosynthesis. *Acc. Chem. Res.* **2009**, *42*, 1890−1898.

(4) D'Souza, F.; Smith, P. M.; Zandler, M. E.; McCarty, A. L.; Itou, M.; Araki, Y.; Ito, O. Energy Transfer Followed by Electron Transfer in a Supramolecular Triad Composed of Boron Dipyrrin, Zinc Porphyrin, and Fullerene: A Model for the Photosynthetic Antenna-Reaction Center Complex. *J. Am. Chem. Soc.* **2004**, *126*, 7898−7907.

(5) Balzani, V.; Bolletta, F.; Gandolfi, M. T.; Maestri, M. Excited States Redox Reactions. *Top. Curr. Chem.* **1978**, *75*, 1−64.

(6) Wiehe, A.; Senge, M. O.; Schafer, A.; Speck, M.; Tannert, S.; Kurreck, H.; Roder, B. Electron Donor−Acceptor Compounds: Exploiting the Triptycene Geometry for the Synthesis of Porphyrin Quinone Dyads, Triads, and a Tetrad. *Tetrahedron* **2001**, *57*, 10089−10110.

(7) Koyama, Y.; Miki, T.; Wang, X.-F.; Nagae, H. Dye-Sensitized Solar Cells Based on the Principles and Materials of Photosynthesis: Mechanisms of Suppression and Enhancement of Photocurrent and Conversion Efficiency. *Int. J. Mol. Sci.* **2009**, *10*, 4575−4622.

(8) Bai, D.; Beeniston, A. C.; Hagon, J.; Lemmetyinen, H.; Tkachenko, N. V.; Clegg, W.; Harrington, R. W. Exploring Förster Electronic Energy Transfer in a Decoupled Anthracenyl-Based Borondipyrromethene (BODIPY) Dyad. *Phys. Chem. Chem. Phys.* **2012**, *14*, 4447−4456.

(9) Liu, J. Y.; El-Kously, M. E. E. -L.; Fukuzumi, S.; Ng, D. K. P. Mimicking Photosynthetic Antenna-Reaction-Center Complexes with a (Boron Dipyrromethene)$_3$−Porphyrin−C_{60} Pentad. *Chem.—Eur. J.* **2011**, *17*, 1605−1613.

(10) Vijendra, S. S.; Mangalampalli, R. Supramolecular Tetrads Containing Sn(IV) Porphyrin, Ru(II) Porphyrin, and Expanded Porphyrins Assembled Using Complementary Metal−Ligand Interactions. *Inorg. Chem.* **2011**, *50*, 1713−1722.

(11) Jing, B.; Zhu, D. Fullerene−Fluorescein−Anthracene Hybrids: A Model for Artificial Photosynthesis and Solar Energy Conversion. *Tetrahedron Lett.* **2004**, *45*, 221−224.

(12) Flamigni, L.; Talarico, A.; Gunter, M. J.; Johnston, M. R.; Jeynes, T. P. Photoinduced Electron Transfer in Paraquat Inclusion Complexes of Porphyrin-Based Receptors. *New J. Chem.* **2003**, *27*, 551−559.

(13) Flamigni, L.; Johnston, M. R.; Giribabu, L. Photoinduced Electron Transfer in Bisporphyrin−Diimide Complexes. *Chem.—Eur. J.* **2002**, *8*, 3938−3947.

(14) Jono, R.; Yamashita, K. Two Different Lifetimes of Charge Separated States: A Porphyrin−Quinone System in Artificial Photosynthesis. *J. Phys. Chem. C* **2012**, *116*, 1445−1449.

(15) Zhao, P.; Huang, J.-W.; Xu, L.-C.; Ma, L.; Ji, L.-N. The Photoinduced Electron Transference of Porphyrin−Anthraquinone Dyads Bridged with Different Lengths of Links. *Spectrochim. Acta, Part A* **2011**, *78*, 437−442.

(16) Tao, M.; Liu, L.; Liu, D.; Zhou, X. Photoinduced Energy and Electron Transfer in Porphyrin-Anthraquinone Dyads Bridged with a Triazine Group. *Dyes Pigments* **2010**, *85*, 21−26.

(17) Kumar, P. P.; Premaladha, G.; Maiya, B. G. Porphyrin−Anthraquinone Dyads: Synthesis, Spectroscopy and Photochemistry. *J. Chem. Sci.* **2005**, *117*, 193−201.

(18) Williams, D. A.; Bowler, B. E. Porphyrin to Quinone Electron Transfer Across a Depsipeptide which Forms an α-Helical Turn. *Inorg. Chim. Acta* **2000**, *297*, 47−55.

(19) Shibano, Y.; Sasaki, M.; Tsuji, H.; Araki, Y.; Ito, O.; Tamao, K. Conformation Effect of Oligosilane Linker on Photoinduced Electron Transfer of Tetrasilane-Linked Zinc Porphyrin−[60]Fullerene Dyads. *J. Organomet. Chem.* **2007**, *692*, 356−367.

(20) Marcus, R. A. Electron Transfer Reactions in Chemistry: Theory and Experiment. *Angew. Chem., Int. Ed.* **1993**, *32*, 1111−1121.

(21) Schuster, D. I.; MacMahon, S.; Guldi, D. M.; Echegoyen, L.; Braslavsky, S. E. Synthesis and photophysics of porphyrin−fullerene donor−acceptor dyads with conformationally flexible linkers. *Tetrahedron* **2006**, *62*, 1928−1936.

(22) Okamoto, K.; Fukuzumi, S. Hydrogen Bonds Not Only Provide a Structural Scaffold to Assemble Donor and Acceptor Moieties of Zinc Porphyrin−Quinone Dyads but Also Control the Photoinduced Electron Transfer to Afford the Long-Lived Charge-Separated States. *J. Phys. Chem. B* **2005**, *109*, 7713−7723.

(23) Wasielewski, M. R. Photoinduced Electron Transfer in Supramolecular Systems for Artificial Photosynthesis. *Chem. Rev.* **1992**, *92*, 435−461.

(24) Kandhadi, J.; Kanaparthi, R. K.; Giribabu, L. Germanium(IV) Phthalocyanine-Porphyrin Based Hetero Trimers: Synthesis, Spectroscopy and Photochemistry. *J. Porphyrins Phthalocyanines* **2012**, *16*, 282−289.

(25) Giribabu, L.; Kumar, C. V.; Reddy, P. Y. Axial-Bonding Heterotrimers Based on Tetrapyrrolic Rings: Synthesis, Characterization, and Redox and Photophysical Properties. *Chem. Asian J.* **2007**, *2*, 1574−1580.

(26) Reeta, P. S.; Kanaparthi, R. K.; Giribabu, L. β-Pyrrole Substituted Porphyrin-Pyrene Dyads Using Vinylene Spacer: Synthesis, Characterization and Photophysical Properties. *J. Chem. Sci.* **2013**, *125*, (0000).

(27) Fuhrhop, J. H.; Smith, K. M. *In Porphyrins and Metalloporphyrins*; Smith, K. M., Ed.; Elsevier: Amsterdam, 1975; p 769.

(28) Bonfantini, E. E.; Burrell, A. K.; Campbell, W. M.; Crossley, M. J.; Gosper, J. J.; Harding, M. M.; Officer, D. L.; Reid, D. C. W. Efficient synthesis of Free-Base 2-Formyl-5,10,15,20-Tetraarylporphyrins, Their Reduction and Conversion to [(Porphyrin-2-yl)methyl]phosphonium Salts. *J. Porphyrins Phthalocyanines* **2002**, *6*, 708−719.

(29) Giribabu, L.; Kumar, C. V.; Reddy, V. G.; Reddy, P. Y.; Rao, Ch. S.; Jang, S. -R.; Yum, J. -H.; Nazeeruddin, M. K.; Gratzel, M. Unsymmetrical Alkoxy Zinc Phthalocyanine for Sensitization of Nanocrystalline TiO_2 Films. *Sol. Energy Mater. Sol. Cells* **2007**, *91*, 1611−1617.

(30) Frisch, M. J.; Trucks, G. W.; Schlegel, H. B.; Scuseria, G. E.; Robb, M. A.; Cheeseman, J. R.; Scalmani, G.; Barone, V.; Mennucci, B.; Petersson, G. A. et al. *Gaussian 09, Revision A.01*; Gaussian, Inc.: Wallingford, CT, 2009.

(31) Quimby, D. J.; Longo, F. R. Luminescence Studies on Several Tetraarylporphins and Their Zinc Derivatives. *J. Am. Chem. Soc.* **1975**, *97*, 5111−5117.

(32) Rodriguez, J.; Kirmaier, C.; Holten, D. Optical Properties of Metalloporphyrin Excited States. *J. Am. Chem. Soc.* **1989**, *111*, 6500−6506.

(33) Fukuzumi, S.; Endo, Y.; Kashiwagi, Y.; Araki, Y.; Ito, O.; Imahori, H. Novel Photocatalytic Function of Porphyrin-Modified Gold Nanoclusters in Comparison with the Reference Porphyrin Compound. *J. Phys. Chem. B* **2003**, *107*, 11979−11986.

(34) Reeta, P. S.; Kandhadi, J.; Giribabu, L. One-pot Synthesis of β-Carboxy Tetra Aryl Porphyrins: Potential Applications to Dye-Sensitized Solar Cells. *Tetrahedron Lett.* **2010**, *51*, 2865−2867.
(35) Giribabu, L.; Kumar, C. V.; Reddy, P. Y. Porphyrin-Rhodanine Dyads for Dye Sensitized Solar Cells. *J. Porphyrins Phthalocyanines* **2006**, *10*, 1007−1016.
(36) James R. Bolton, J. R.; Ho, T.-F.; Liauw, S.; Aleksander Siemiarczuk, A.; Calvin S. K. Wan, C. S. K.; Weedon, A. C. Light-induced Intramolecular Electron Transfer from a Porphyrin linked to a *p*-Benzoquinone by a Rigid Spacer Group. *J. Chem. Soc., Chem. Commun.* **1985**, 559−560 and references therein..
(37) Barber, D. C.; Frietag, R. A.; Whitten, D. G. Atropisomer-specific formation of premicellar porphyrin J-aggregates in aqueous surfactant solutions. *J. Phys. Chem.* **1991**, *95*, 4074−4086.
(38) Excited-state singlet state energy levels (E_{0-0}) of H_2L^1, ZnL^1, AQ-$(H_2)_2$, and AQ-$(Zn)_2$ are 1.96, 2.05, 1.85, and 1.96 eV, respectively.
(39) Bolton, J. R.; Schmidt, J. A.; Ho, T. F.; Liu, J. -Y.; Roach, K. R.; Weedon, A. C.; Archer, M. D.; Wilford, J. H.; Gadzekpo, V. P. Y. *Electron transfer in Inorganic, Organic and Biological Systems*; American Chemical Society: Washington, DC, 1991; Chapter 7.
(40) Korth, O.; Wiehe, A.; Kurreck, H.; Roder, B. Photoinduced Intramolecular Electron Transfer in Covalently Linked porphyrin−Triptycene−Bis/quinone Diads and Triads. *Chem. Phys.* **1999**, *246*, 363−372.
(41) Brookfield, R. L.; Ellul, H.; Harriman, A.; Porter, G. Luminescence of Porphyrins and Metalloporphyrins. Part 11. Energy Transfer in Zinc−Metal-Free Porphyrin Dimers. *J. Chem. Soc., Faraday Trans. 2* **1986**, *82*, 219−233.
(42) Sakata, Y.; Nishitani, S.; Nishimizu, N.; Misumi, S. Synthesis of a Model Compound for the Photosynthetic Electron Transfer. *Tetrahedron Lett.* **1985**, *26*, 5207−5210.
(43) Karr, P. A.; Zandler, M. E.; Beck, M.; Jaeger, J. D.; McCarty, A. L.; Smith, P. M.; D'Souza, F. Predicting the Site of Electron Transfer Using DFT Frontier Orbitals: Studies on Porphyrin Attached Either to Quinone or Hydroquinone, and Quinhydrone Self-Assembled Supramolecular Complexes. *J. Mol. Struct. Theochem.* **2006**, *765*, 91−103.
(44) Paddon-Row, M. N. Some Aspects of Orbital Interactions Through Bonds: Physical and Chemical Consequences. *Acc. Chem. Res.* **1982**, *15*, 245−251.
(45) Anderson, P. W. Antiferromagnetism. Theory of Superexchange Interaction. *Phys. Rev.* **1950**, *79*, 350−356.
(46) Won, Y.; Friesner, R. A. On the Viability of the Superexchange Mechanism in the Primary Charge Separation Step of Bacterial Photosynthesis. *Biochim. Biophys. Acta, Bioenerg.* **1988**, *935*, 9−18.